Chinese Chemical Letters 34 (2023) 108231

Contents lists available at ScienceDirect

Chinese Chemical Letters

journal homepage: www.elsevier.com/locate/cclet

Environmentally sensitive fluorescent probes with improved properties for detecting and imaging PDEδ in live cells and tumor slices

Keliang Li[a,1], Shanchao Wu[a,1], Gaopan Dong[b,1], Yu Li[a], Wei Wang[a], Guoqiang Dong[a], Zhanying Hong[a,*], Minyong Li[b,*], Chunquan Sheng[a,*]

[a] School of Pharmacy, Second Military Medical University, Shanghai 200433, China
[b] Department of Medicinal Chemistry, Key Laboratory of Chemical Biology (MOE), School of Pharmaceutical Sciences, Cheeloo College of Medicine, Shandong University, Ji'nan 250012, China

ARTICLE INFO

Article history:
Received 6 December 2022
Revised 4 February 2023
Accepted 13 February 2023
Available online 16 February 2023

Keywords:
Antitumor
PDEδ
Fluorescent probes
Environmentally sensitive
Binding affinity

ABSTRACT

Kirsten rat sarcoma viral oncogene homolog (KRAS)–phosphodiesterase-delta (PDEδ) is a promising target for antitumor drug discovery. Herein, highly efficient and environmentally sensitive fluorescent probes of PDEδ (**DS-Probes**) were rationally designed. As compared with the reported PDEδ probes, **DS-Probes** showed higher binding affinity and selectivity, which were able to conveniently and efficiently label PDEδ in live cells as well as tumor tissues. Therefore, these fluorescent probes are expected to facilitate PDEδ-based mechanism elucidation, drug discovery and pathologic diagnosis.

Pancreatic cancer is associated with high mortality with five-year survival less than 10% [1–3]. Kirsten rat sarcoma viral oncogene homolog (KRAS) has the highest mutation rate (90%) in pancreatic cancer, which is the main factor responsible for the occurrence and development of pancreatic cancer [3–5]. Targeting KRAS signaling has become an important field in antitumor drug discovery and achieved great success [6–10]. In 2021, the first KRAS inhibitor sotorasib was approved for the treatment of non-small-cell lung cancers with KRAS G12C mutations [11]. However, monotherapy of sotorasib is limited due to the low proportion of G12C mutations in all KRAS mutations [12]. Therefore, the development of pan-KRAS inhibitors targeting multiple KRAS mutants is becoming a promising strategy [13].

Phosphodiesterase-delta (PDEδ) plays an important role in regulating the functions of KRAS [8], which assists the transport of KRAS to cell membrane by binding the farnesyl group of KRAS, thereby promoting the activation of downstream signaling pathways [14–16]. Disruption of KRAS–PDEδ protein–protein interaction is a new strategy for drug development targeting mutant KRAS [16,17]. Nevertheless, it is disappointing that the existing PDEδ inhibitors were generally limited by low anti-tumor efficacy and poor selectivity [17,18]. Thus, new chemical tools targeting PDEδ are urgently needed to understand the biological functions and druggability of PDEδ.

In recent years, the visualization of target protein functions by fluorescent probes has facilitated the elucidation of biological mechanisms and drug discovery [20,21]. Fluorescent imaging has the advantages of low invasiveness, low radiation, low toxicity, and fast spatiotemporal localization [22–26]. Small molecule fluorescent probes have become indispensable tools in the fields of molecular biology and medicine [27,28]. Particularly, environment-sensitive fluorescent probes have enhanced fluorescence in hydrophobic environment, showing a significant improvement in the signal-to-noise ratio after target binding and consequently label the target proteins more clearly, providing effective visualization tools for protein function research [29–31].

Currently, three types of chemical fluorescent probes targeting PDEδ have been reported [16,19,32]. Based on PDEδ binder atorvastatin, Waldmann's group designed a fluorescein-labeled atorvastatin probe (**AT-Probe**, Fig. 1A) to detect fluorescence properties (FP) and develop assays [16]. Additionally, they developed benzenedisulfonamide-based probe (**BZ-Probe**, Fig. 1A) with higher selectivity and better binding ability to PDEδ, whereas it failed to possess environmental sensitivity [19].

In our previous studies, the first class of environment-sensitive fluorescent probes (**QZ-Probes**, Fig. 1A) were designed to image

* Corresponding authors.
E-mail addresses: hongzhy001@163.com (Z. Hong), mli@sdu.edu.cn (M. Li), shengcq@smmu.edu.cn (C. Sheng).
[1] These authors contributed equally to this work.

https://doi.org/10.1016/j.cclet.2023.108231
1001-8417/

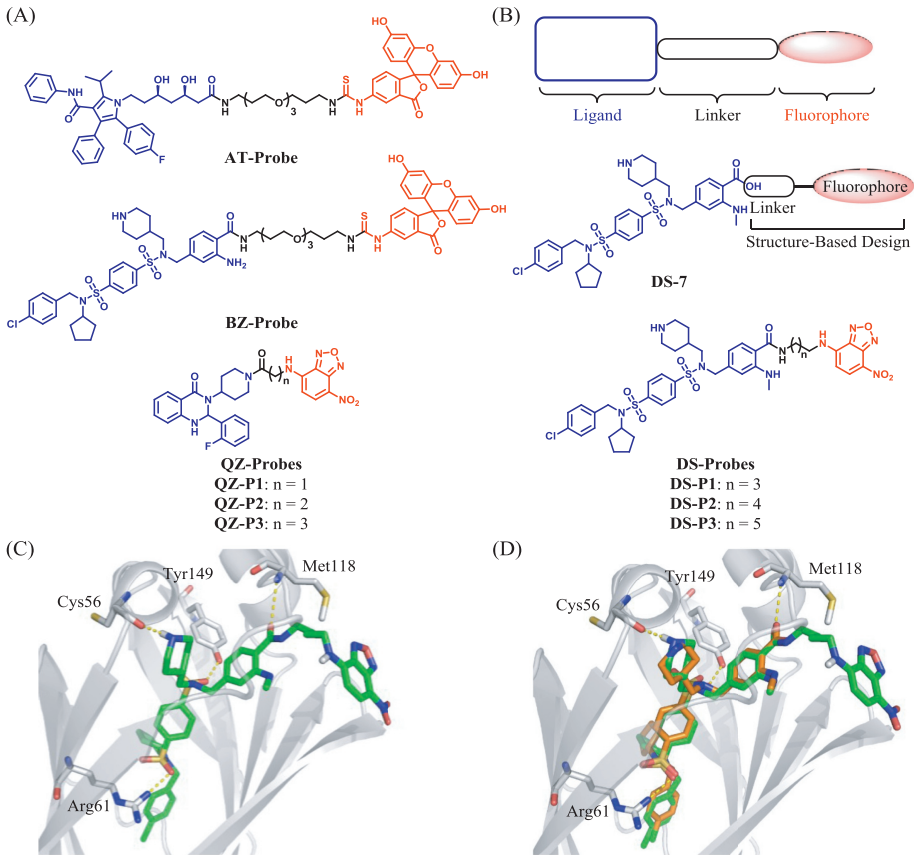

Fig. 1. Design rationale of environment-sensitive fluorescent probes of PDEδ. (A) Chemical structures of the reported PDEδ fluorescent probes. (B) The design strategy of **DS-Probes**. (C) The binding mode of **DS-P1** (green) with PDEδ. (D) The superimposed conformation of the ligand (orange) with **DS-P1**.

PDEδ in Capan-1 and MIA PaCa-2 pancreatic cancer cells and tissues [32]. Nevertheless, **QZ-Probes** had weak binding activity to PDEδ (K_D = 440–682 nmol/L). Only when the concentration of PDEδ was higher than 0.5 μmol/L, the fluorescence signal could be significantly enhanced. To overcome this limitation, herein, more effective PDEδ environment-sensitive fluorescent probes were designed and synthesized.

To improve the binding affinity, highly active PDEδ inhibitors were required to be attached with fluorophores. First, the fluorescent groups 7-nitrobenzo-2-oxa-1,3-diazole (NBD) with alkyl chains, which possessed environmental sensitivity, good water-solubility and small size were used [33]. Then, among the PDEδ inhibitors, benzenedisulfonamides showed the highest binding activity to PDEδ, which antagonized the allosteric effect of PDEδ mediated by Arl2 [19]. On the basis of excellent binding activity, benzenedisulfonamide PDEδ inhibitor **DS-7** (K_D < 2 nmol/L, Fig. 1B) was selected to design novel fluorescent probes of PDEδ. The binding mode of compound **DS-7** with PDEδ reveals that its terminal carboxyl group is located in the Tyr149 pocket and forms hydrogen bonding interaction with Met118 (PDB code: 5ML4) [19]. Notably, this group also points to the outside of the binding pocket, offering a favorable site for probe design. Thus, the carboxyl group of compound **DS-7** was extended by an alkyl side chain and subsequently connected with NBD, affording three new PDEδ fluorescent probes (herein named **DS-Probes**, Fig. 1B).

Next, in order to clarify the binding mode of **DS-Probes** with PDEδ, **DS-P1** (Fig. 1B) was selected for molecular docking and the results indicated that the newly designed probe maintained the binding mode of the ligand and key hydrogen bonds with Cys56, Arg61, Met118 and Tyr149 were retained (Fig. 1C). Furthermore, the fluorophores had no interactions with the residues of PDEδ, which had little effect on the binding affinities of **DS-Probes**. As shown in the superimposed structures (Fig. 1D), the binding mode of **DS-P1** was highly similar to that of ligand **DS-7**, which validated the rationality of the probe design.

The synthetic route of **DS-Probes** (**DS-P1**, **DS-P2**, **DS-P3**) is shown in Scheme 1. Starting from compound **1** (NBD-Cl), NBD fluorescent fragments **3** was prepared by substitution reaction with diamines followed by removing the Boc protection, which can be used directly without further purification. Using cyclopentylamine and *p*-chlorobenzaldehyde as starting materials, intermediate **6** was obtained through reductive amination reaction, and then condensed with *p*-bromobenzenesulfonyl chloride to obtain intermediate **7**. Compound **7** was coupled with benzylthiol under the catalysis of metal palladium to afford intermediate **8**, which was further oxidized by dichlorohydantoin to give key intermediate **9**. Compound **10** was substituted by methylamine hydrochloride to obtain intermediate **11**, which was further converted to intermediate **12** *via* reductive amination reaction with 1-Boc-4-(aminomethyl)piperidine. Then, compound **12** was condensed with key intermediate **9** to give intermediate **13**. After hydrolysis of compound **13** with lithium hydroxide (LiOH), the demethylated compound **14** was condensed with key intermediate **3** in the presence of *O*-benzotriazol-1-yl-tetramethyluronium hexafluorophosphate (HBTU) and triethylamine (TEA). Finally, the target compounds **DS-Probes** were obtained after removing the protective group of the compound **14**.

Initially, the PDEδ-binding activities of **DS-Probes** were assayed by FP and surface plasmon resonance (SPR) methods using PDEδ inhibitor **Deltazinone 1** and our previously reported probe **QZ-P1** as positive controls (Table S1 in Supporting information). In the FP assay, all the three probes showed potent activi-

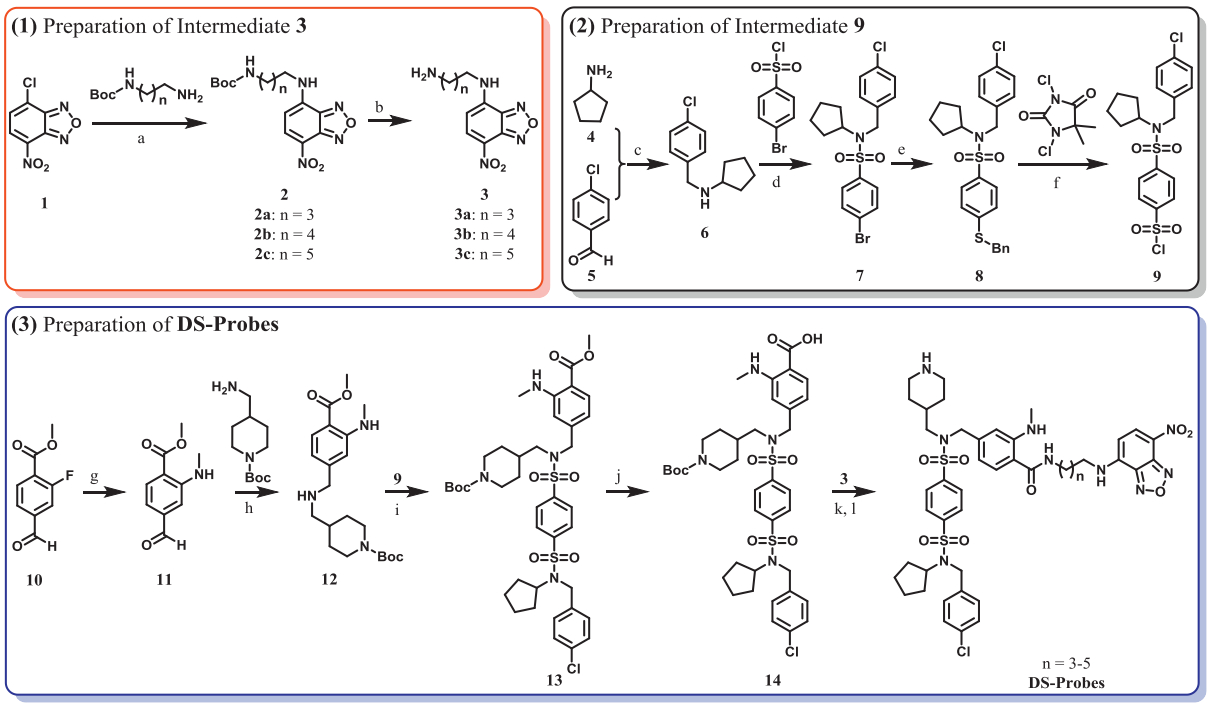

Scheme 1. Synthesis of **DS-Probes**. Reagent and conditions: a) DIPEA, NMP, microwave, 110 °C, 1.5 h, 70%–87%; b) TFA, DCM, r.t., 0.5 h; c) $MgSO_4$, $NaBH_4$, MeOH, r.t., 14 h, 97%; d) TEA, DCM, 40 °C, 12 h, 69%; e) benzyl mercaptan, $Pd_2(dba)_3$, X-Phos, DIPEA, 1,4-dioxane, 110 °C, 12 h, 75%; f) MeCN-AcOH-H_2O, 0 °C, 2 h, 76%; g) K_2CO_3, $MeNH_3Cl$, NMP, 100 °C, 24 h, 52%; h) $NaBH(OAc)_3$, AcOH, 1,2-dichloroethane, r.t., overnight, 60%; i) TEA, DCM, 0 °C, 1 h, 85%; j) LiOH, THF-MeOH-H_2O, 50 °C, 1 h, 85%; k) HBTU, TEA, DMF, r.t., 2 h; l) TFA, DCM, r.t., 0.5 h, 35%–39%.

Table 1
Spectral properties of **DS-Probes**.

Probe	λ_{max} (nm)	λ_{ex} (nm)	λ_{em} (nm)	Φ (%)			
				PBS	DMSO	0.125 μmol/L PDEδ	0.25 μmol/L PDEδ
DS-P1	354/480	344/470	525	0.098	7.27	29.4	34.4
DS-P2	355/486	337/477	535	0.071	13.99	18.0	38.0
DS-P3	355/485	324/468	521	0.075	23.08	19.0	37.0

ties in binding PDEδ (K_D range: 16.08–34.17 nmol/L), which were significantly more potent than probe **QZ-P1** ($K_D = 682$ nmol/L). The SPR assay further confirmed the PDEδ binding ability of the probes (K_D range: 0.061–0.25 μmol/L). **DS-P1** was proven to be the most potent probe in both assays (FP, $K_D = 16.08$ nmol/L; SPR, $K_D = 0.061$ μmol/L).

The *in vitro* antitumor activity of the probes was further assayed against KRAS-dependent pancreatic cancer cell lines MIA PaCa-2 and Capan-1 using the cell counting kit-8 (CCK-8) method. As shown in Table S1, **DS-Probes** exhibited moderate antiproliferation activity against MIA PaCa-2 cell line (IC_{50} range: 15.8–18.3 μmol/L) and Capan-1 cell line (IC_{50} range: 17.6–31.3 μmol/L), which were suitable for cellular imaging.

Then, the spectra of **DS-Probes** were measured (Fig. S2 in Supporting information). The maximum absorption wavelength (λ_{max}), maximum excitation wavelength (λ_{ex}) and maximum emission wavelength (λ_{em}) are shown in Table 1. The difference between λ_{ex} and λ_{em} indicated that the probes had favorable properties for fluorescence detection.

Furthermore, the fluorescence quantum yields (Φ) of the probes were measured (Table 1). In the phosphate buffered solution (PBS, pH 7.4), the fluorescence quantum yields of **DS-Probes** were less than 0.1%, while the fluorescence quantum yields of the probes were significantly increased in dimethyl sulfoxide (DMSO, 7.27%–23.08%). These results suggested that **DS-Probes** possessed the environmentally sensitive turn-on mechanism. Interestingly, PDEδ was tested as non-fluorescent in our previous works [32], the addition of a little amount of PDEδ (0.125 μmol/L), also led to significant enhancement of the fluorescence quantum yields. With the increase of protein concentration, the fluorescence quantum yields were further increased in a concentration-depended manner (Table 1). Similarly, the fluorescence intensity of the probes also depended on the concentration of PDEδ (Fig. 2). In contrast, the fluorescence intensity of **QZ-P1** was not obviously increased in the presence of the low concentration of PDEδ (0.125 μmol/L). These results indicated that **DS-Probes** had good environmental sensitivity to PDEδ, which were significantly more effective than probe **QZ-P1**.

To verify that the **DS-Probes** act on PDEδ in cells, the effects of different probes on the thermal stability of PDEδ in MIA PaCa-2 cells were investigated by cellular thermal shift assays. After the treatment of probes (20 μmol/L) for 2 h, the cell samples were collected and divided into 10 groups. Then, the changes of PDEδ in each group were detected by the Western blot at different temperatures. The results revealed that the thermal stability of PDEδ was significantly improved after the treatment of **DS-Probes** when compared with the blank control (Fig. S3A in Supporting information). When the temperature was above 55 °C, the PDEδ bands of the **DS-Probes** were still clearly visible. The **DS-P1** group showed the highest stability, and there was still a little amount of PDEδ at 70 °C. In contrast, the bands in the **QZ-P1** group and the blank control group (1% DMSO) gradually disappeared above 52 °C. The

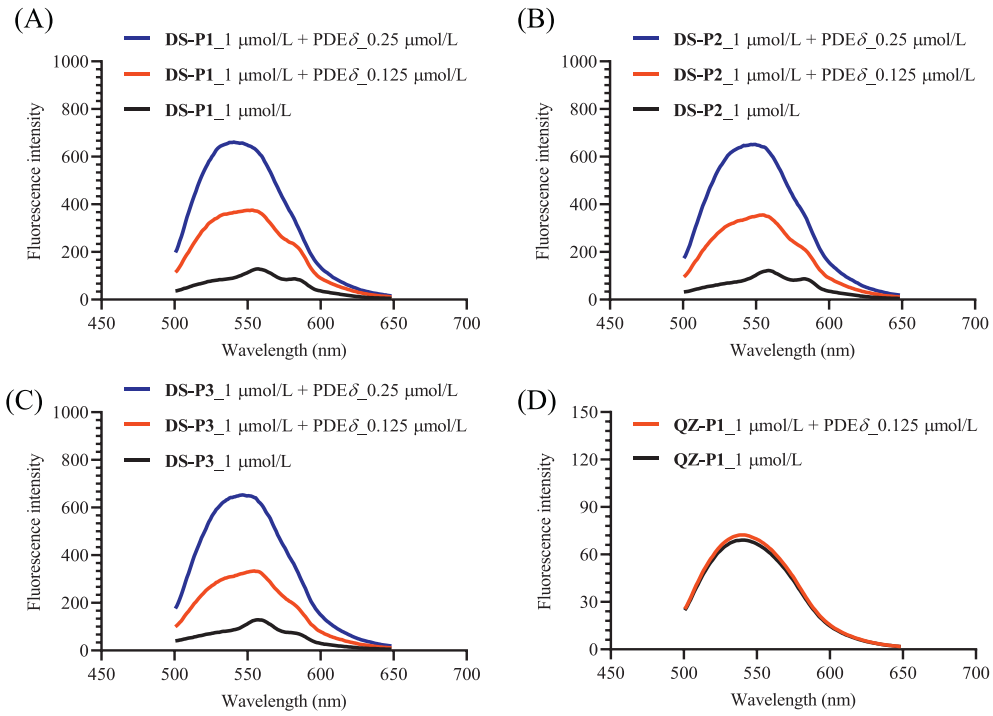

Fig. 2. Fluorescence emission spectra of **DS-Probes** and **QZ-P1** before and after the addition of PDEδ. (A) **DS-P1**; (B) **DS-P2**; (C) **DS-P3**; (D) **QZ-P1**.

results indicated that **DS-Probes** were able to bind PDEδ in cells, which were significantly more effective than probe **QZ-P1**.

In order to clarify the effects of **DS-Probes** on the KRAS signaling pathway in cells, the changes of the phosphorylation levels of protein kinase B (Akt) and extracellular signal-related kinase (Erk) in the downstream signaling pathways in MIA PaCa-2 cell line were evaluated by Western blot analysis. After the treatment of **DS-Probes** for 6 h, the phosphorylation levels of Akt and Erk were separately down-regulated by **DS-Probes** and **DS-P3**. Furthermore, **DS-P1** and **DS-P2** affected Akt and **DS-P3** affected Erk in a concentration-dependent manner (Fig. S3B in Supporting information). At the same concentration, the down-regulation effects of **DS-Probes** on Akt were more obvious than those observed in **Deltazinone 1** and **QZ-P1** groups. These results suggested that **DS-Probes** acted on PDEδ in MIA PaCa-2 cells, interfered with KRAS–PDEδ interaction, and affected the KRAS signaling pathway.

At present, specific fluorescent probes are valuable tools for visualizing the expression and localization of target proteins in cells [34,35]. Based on the excellent fluorescence properties, **DS-Probes** were used to detect and image PDEδ in KRAS-dependent MIA PaCa-2 cells. The results showed that **DS-Probes** (5 μmol/L) rapidly bound to PDEδ, enabling PDEδ imaging in live cells, among which the fluorescence of **DS-P1** was relatively stronger (Fig. 3A). For the fluorescence distribution, green fluorescence was mainly distributed in the cytoplasm and plasma membrane, where PDEδ was mainly located (Fig. 3A). Furthermore, MIA PaCa-2 cell line was co-incubated with 5 μmol/L **DS-Probes** and 100 μmol/L **DS-7**. The results showed that the fluorescence intensity of the probes was decreased by the competition of PDEδ inhibitor **DS-7**, indicating that **DS-Probes** can reversibly bind to PDEδ. When **DS-Probes** (5 μmol/L) were evaluated in the normal HEK-293T cell line, the results showed that probes failed to stain cells, indicating that **DS-Probes** can selectively bind to PDEδ. These results demonstrated that **DS-Probes** can be used as effective tools for real-time detection and rapid visualization of KRAS–PDEδ protein–protein interaction in live cells. The imaging results of Capan-1 cells were also consistent with those observed in MIA PaCa-2 cell images (Figs. S4–S6 in Supporting information).

The staining effect of **DS-Probes** to MIA PaCa-2 cell line was further quantitatively analyzed by flow cytometry (FCM). As shown in Fig. 3B, the fluorescence intensity of MIA PaCa-2 incubated with 5 μmol/L probes was significantly stronger than that of MIA PaCa-2 incubated with 100 μmol/L **DS-7** and that of the control group. When the probes were competed with 100 μmol/L **DS-7**, the fluorescence intensity of cells was significantly reduced. The results further demonstrated the staining effect and selectivity of **DS-Probes**. The FCM results of Capan-1 cells were also consistent with those observed in MIA PaCa-2 cells (Fig. S7 in Supporting information).

Additionally, the effects of **DS-Probes** on PDEδ in tumor tissues were further detected by fluorescence staining of tissue sections. Tumor tissue sections of the Capan-1 cell line were stained with probes at a concentration of 5 μmol/L, and **DS-7** (100 μmol/L) was used as a competitive ligand to investigate the reversibility and specificity of probes in imaging PDEδ. As shown in Fig. 3C, the tumor slices treated with the probes alone had a good response of green fluorescence, among which the fluorescence of **DS-P1** and **DS-P3** was relatively stronger. In contrast, the fluorescence intensity of normal mice skin tissue slices treated with **DS-Probes** (5 μmol/L) was relatively weaker than that in Capan-1 tumor slices. In the competitive binding experiment, the fluorescence intensity was significantly reduced when high concentration (100 μmol/L) of **DS-7** was added, which further proved that the probes reversibly and selectively bound to PDEδ and labeled tumor cells in tissues. The experimental procedures and the animal use and care protocols were approved by the Committee on Ethics of Biomedicine, Second Military Medical University.

In summary, a new series of environmentally sensitive fluorescent probes for PDEδ was rationally designed. **DS-Probes** had stronger affinity, better selectivity and higher sensitivity to PDEδ, leading to better imaging capabilities. Mechanism studies revealed that **DS-Probes** could selectively bind to PDEδ and down-regulate the phosphorylation levels of Erk and Akt in the KRAS signaling

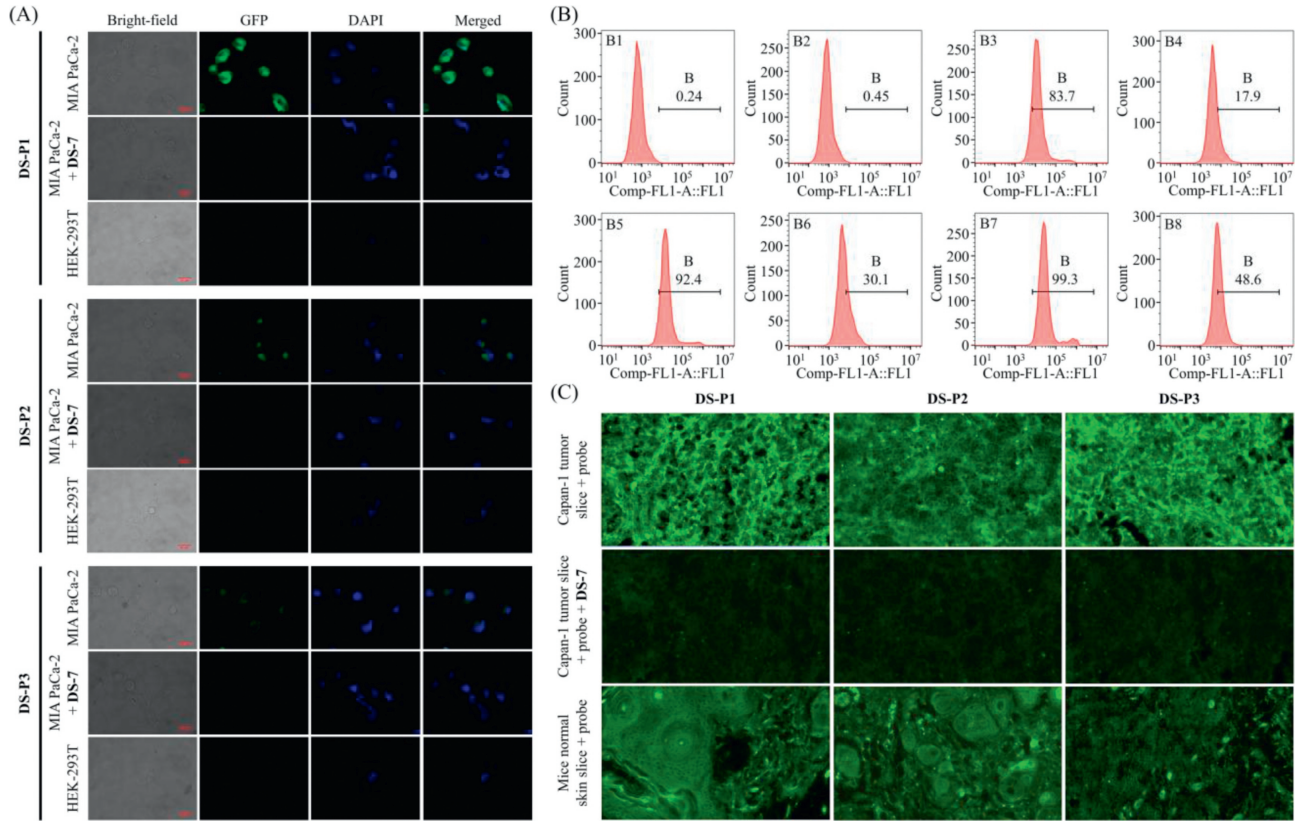

Fig. 3. Fluorescence labeling of **DS-Probes** in tumor cells and tissues. (A) Fluorescence images of MIA PaCa-2 and HEK-293T cell lines incubated with **DS-Probes**. Scale bar = 67 μm. (B) Flow cytometry results of **DS-Probes** in MIA PaCa-2 cells. B1: control (1% DMSO); B2: 100 μmol/L **DS-7**; B3: 5 μmol/L **DS-P1**; B4: 5 μmol/L **DS-P1** + 100 μmol/L **DS-7**; B5: 5 μmol/L **DS-P2**; B6: 5 μmol/L **DS-P2** + 100 μmol/L **DS-7**; B7: 5 μmol/L **DS-P3**; B8: 5 μmol/L **DS-P3** + 100 μmol/L **DS-7** (Meaning of the figures in B1–B8: a ratio of the area under the horizontal line at a fixed position to the total area under the curve in percent). (C) Fluorescence staining of Capan-1 cell xenograft sections by **DS-Probes**. The slices were captured by the OLYMPUS VS120 virtual slide microscope (objective lens: 40×).

pathway. Furthermore, **DS-Probes** quickly, efficiently, selectively and reversibly labeled PDEδ in living cells and tumor tissues. Thus, **DS-Probes** are expected to serve as valuable tools for the detection and visualization of KRAS–PDEδ interaction with potential to be applicated in better understanding the biological functions of PDEδ and developing assays for drug screening. Admittedly, fluorescence imaging of PDEδ was limited to tumor cells and tissues due to the spectral properties of **DS-Probes**, the further optimization of PDEδ-labeling probes is currently underway in our groups.

Declaration of competing interest

The authors declare that they have no known competing financial interests or personal relationships that could have appeared to influence the work reported in this paper.

Acknowledgments

This work was supported by the National Key Research and Development Program of China (No. 2020YFA0509200 to C. Sheng), National Natural Science Foundation of China (Nos. 81903436 to Y. Li, 82204211 to W. Wang and 22077138 to S. Wu) and Shanghai Rising-Star Program (No. 22QA1411300 to S. Wu).

Supplementary materials

Supplementary material associated with this article can be found, in the online version, at doi:10.1016/j.cclet.2023.108231.

References

[1] J. Gillson, Y. Ramaswamy, G. Singh, et al., Cancers 12 (2020) 1341.
[2] W. Zhang, K. Zhang, P. Zhang, et al., Front. Oncol. 10 (2020) 604531.
[3] Z. Zhu, S. Xiao, H. Hao, Q. Hou, X. Fu, Curr. Top. Med. Chem. 19 (2019) 2176–2186.
[4] S.M. Gomes-Filho, S.E. Dos, E. Bertoldi, et al., Cell. Oncol. 43 (2020) 445–460.
[5] M. Wang, Z. Guo, J. Zeng, et al., Chin. Chem. Lett. 34 (2023) 107651.
[6] T. Maurer, L.S. Garrenton, A. Oh, et al., Proc. Natl. Acad. Sci. U. S. A. 109 (2012) 5299–5304.
[7] N. Berndt, A.D. Hamilton, S.M. Sebti, Nat. Rev. Cancer 11 (2011) 775–791.
[8] S.A. Ismail, Y.X. Chen, A. Rusinova, et al., Nat. Chem. Biol. 7 (2011) 942–949.
[9] B. Bournet, C. Buscail, F. Muscari, P. Cordelier, L. Buscail, Eur. J. Cancer 54 (2016) 75–83.
[10] Q. Sun, J.P. Burke, J. Phan, et al., Angew. Chem. Int. Ed. 51 (2012) 6140–6143.
[11] C. Sheridan, Nat. Biotechnol. 39 (2021) 1032–1034.
[12] A.D. Cox, S.W. Fesik, A.C. Kimmelman, J. Luo, C.J. Der, Nat. Rev. Drug Discov. 13 (2014) 828–851.
[13] M.B. Ryan, R.B. Corcoran, Nat. Rev. Clin. Oncol. 15 (2018) 709–720.
[14] H. Zhang, X.H. Liu, K. Zhang, et al., J. Biol. Chem. 279 (2004) 407–413.
[15] A. Chandra, H.E. Grecco, V. Pisupati, et al., Nat. Cell Biol. 14 (2011) 148–158.
[16] G. Zimmermann, B. Papke, S. Ismail, et al., Nature 497 (2013) 638–642.
[17] B. Papke, S. Murarka, H.A. Vogel, et al., Nat. Commun. 7 (2016) 11360.
[18] J. Cheng, Y. Li, X. Wang, G. Dong, C. Sheng, J. Med. Chem. 63 (2020) 7892–7905.
[19] P. Martín-Gago, E.K. Fansa, C.H. Klein, et al., Angew. Chem. Int. Ed. 56 (2017) 2423–2428.
[20] J. Xing, Q. Gong, O.U. Akakuru, et al., Nanoscale 12 (2020) 24311–24330.
[21] N. Ahmed, W. Zareen, Y. Ye, Chin. Chem. Lett. 33 (2022) 2765–2772.
[22] E. De Boer, N.J. Harlaar, A. Taruttis, et al., Br. J. Surg. 102 (2015) e56–e72.
[23] R.R. Allison, Photodiagnosis Photodyn. Ther. 13 (2016) 73–80.
[24] E. Upchurch, S. Griffiths, G.R. Lloyd, et al., Future Oncol. 13 (2017) 2363–2382.
[25] T. Nagaya, Y.A. Nakamura, P.L. Choyke, H. Kobayash, Front. Oncol. 7 (2017) 314.
[26] Q. Zhou, S. Wang, X. Ran, et al., Chin. Chem. Lett. 34 (2023) 107922.
[27] J.V. Jun, D.M. Chenoweth, E.J. Petersson, Org. Biomol. Chem. 18 (2020) 5747–5763.
[28] M. Staderini, M.A. Martín, M.L. Bolognesi, J.C. Menéndez, Chem. Soc. Rev. 44 (2015) 1807–1819.
[29] Z. Liu, T. Jiang, B. Wang, et al., Anal. Chem. 88 (2016) 1511–1515.

[30] T. Liu, Y. Jiang, Z. Liu, et al., MedChemComm 8 (2017) 1668–1672.
[31] Z. Liu, Z. Miao, J. Li, et al., Chem. Biol. Drug Des. 85 (2015) 411–417.
[32] G. Dong, L. Chen, J. Zhang, et al., Anal. Chem. 92 (2020) 9516–9522.
[33] C. Jiang, H. Huang, X. Kang, et al., Chem. Soc. Rev. 50 (2021) 7436–7495.
[34] R. Dalangin, A. Kim, R.E. Campbell, Int. J. Mol. Sci. 21 (2020) 6197.
[35] Y. Chen, Anal. Biochem. 594 (2020) 113614.